Journal of Polymer Research (2019) 26:208
https://doi.org/10.1007/s10965-019-1875-5

ORIGINAL PAPER

Bio-inspired multiple complementary hydrogen bonds enhance the miscibility of conjugated polymers blended with polystyrene derivatives

Bo-Han Mao[1] · Ahmed F. M. EL-Mahdy[1] · Shiao-Wei Kuo[1,2]

Received: 21 April 2019 / Accepted: 23 July 2019

Abstract
In this study, we prepared bio-inspired multiple-hydrogen-bonded blends of a thymine (T)-functionalized PTC-T conjugated polymer, synthesized through Suzuki coupling polymerization, and an adenine (A)-functionalized polystyrene (PVBA) homopolymer, synthesized through free radical polymerization, in each case applying also alkylene–azide click reactions. The resulting PTC-T/PVBA blends displayed a single glass transition temperature at all blend compositions (as determined using differential scanning calorimetry), suggesting that the miscibility arose because of the strong multiple hydrogen bonding between the A and T groups of the PVBA and PTC-T components, respectively. ^{1}H NMR and FTIR spectroscopy provided evidence for such A–T binary hydrogen bonding in the PTC-T/PVBA miscible domains, both in solution and in the solid state. Furthermore, the incorporation of PVBA into PTC-T affected the photophysical properties of the luminescent film: the physically crosslinked structure formed from the multiple hydrogen bonding interactions improved the quantum yield through phase-miscible behavior.

Keywords Multiple hydrogen bonding · Miscibility · Rod-coil mixture · Conjugated polymer

Introduction

Miscible polymer blends have been studied for at least four decades for their applications in, for example, coatings, fuel cells, solar cells, and electronic devices [1–7]. Because the high molecular weights of polymer blend systems usually lead to small entropies of mixing, miscibility is often imparted by enhancing the enthalpic term through, for example, the introduction of hydrogen bonding interactions [8–11]. Furthermore, relative to random coil polymers, rigid-rod–like polymers are less likely to exhibit miscibility; accordingly, mixtures of rod-like and random coil polymers typically display macrophase-separation behavior, with the random coil polymer excluded from the anisotropic phase due to the entropic part of the mixing free energy [12, 13].

In general, attaching flexible side chain to the rigid-rod polymer enhances their miscibility in blend systems. For example, Heitz et al. grafted polystyrene (PS) onto the side chains of a liquid-crystalline polymer to enhance its miscibility with a PS homopolymer [14]. Another method to improve the miscibility of rod/coil mixtures is the preparation of rod/coil diblock copolymers or graft copolymers through covalent bonding [15–18]. The main drawback of these approaches is that the synthesis of diblock copolymers can be time-consuming and difficult; the miscible blend method is, therefore, preferred for modification of rigid-rod polymers to enhance their flexibility and versatility [19–22].

Conjugated polymers have been investigated widely as functional rigid-rod polymers because of their excellent electrical and optical properties, arising from extensive delocalization of π-electrons and conformational restriction [23–26]. The miscibility of conjugated copolymers is a major factor affecting their photophysical properties and morphological behavior [27, 28]. Vohra et al. prepared polyfluorene blends with PS for use in organic light-emitting diodes; they found, however, that the fluorescence spectrum of the blend system

Electronic supplementary material The online version of this article (https://doi.org/10.1007/s10965-019-1875-5) contains supplementary material, which is available to authorized users.

✉ Shiao-Wei Kuo
kuosw@faculty.nsysu.edu.tw

[1] Department of Materials and Optoelectronic Science, Center of Crystal Research, National Sun Yat-Sen University, Kaohsiung, Taiwan

[2] Department of Medicinal and Applied Chemistry, Kaohsiung Medical University, Kaohsiung 807, Taiwan

Published online: 03 August 2019

did not exhibit any polarization dependence [29]. In addition, Xin et al. used an electrospinning technique to prepare poly(*p*-phenylenevinylene)/polyvinylpyrrolidone blend systems having a beaded fiber morphology [30]; here, the formation of bead structures was induced through phase separation of the random-coil and conjugated polymers. High-affinity bonding—for example, multiple hydrogen bonding—of polymers is another efficient approach toward miscible polymer blends exhibiting desirable physical properties [31–35].

For this study, we selected the PTC copolymer, incorporating triphenyl amine (TPA) and carbazole (Car) units, as our model conjugated polymer. To improve the miscibility of PTC with PS homopolymers, we appended them both with units capable of multiple hydrogen bonding. Accordingly, we used click reactions to synthesize a thymine (T)-functionalized PTC-T conjugated polymer and an adenine (A)-functionalized PVBA homopolymer. The presence of A–T multiple hydrogen bonding can enhance the thermal stability and distinct luminescent properties of polymeric systems in solution. In this study, we used DSC, FTIR and NMR spectroscopy to examine the miscibility and multiple hydrogen bonding of our PTC-T/PVBA blends.

Experimental section

Materials

Styrene, benzoyl peroxide (BPO), propargyl bromide, thymine (T), adenine (A), vinylbenzyl chloride (VBC), copper(I) bromide (CuBr), pentamethyldiethylenetriamine (PMDETA), sodium azide (NaN_3), and K_2CO_3 were purchased from Aldrich. Propargyl adenine (PA), propargyl thymine (PT), poly(vinylbenzyl chloride) (PVBC), and poly(vinylbenzyl azide) ($PVBN_3$) were synthesized as described previously (Scheme 1) [34–38]. 4-Butyl-bis(tetramethyl-dioxaborolane-phenyl)aniline (**2**) and azidohexyl-dibromocarbazole (**5**) were also synthesized as described previously (Scheme 2) [39–41].

PVBA

PA (0.46 g), $PVBN_3$ (0.40 g), and CuBr (0.060 g) were dissolved in dimethylformamide (DMF, 80 mL) and stirred at room temperature. PMDETA (0.14 mL) was added and this mixture was then degassed by three freeze/thaw/pump cycles over 24 h at 60 °C. The sample was passed through the neutral alumina column to remove CuBr. The DMF was evaporated and the residue was stirred in methanol. The solid was filtered off and dried under the vacuum oven to give the PVBA homopolymer as a powder.

PTC-t

A mixture of 2 M aqueous K_2CO_3 (5.4 mL) and THF (8 mL) was added into a mixture of 4-butyl-bis(tetramethyl-dioxaborolane-phenyl)aniline (0.83 g, 1.3 mmol), azidohexyl- dibromocarbazole (0.58 g, 1.3 mol), freshly prepared $Pd(0)(PPh_3)_4$ (0.030 g, 26 mmol), and Aliquat 336® (several drops). The mixture was stirred for 96 h at 65 °C and then poured slowly into the MeOH/H_2O (10:1, *v/v*). The precipitated copolymer was collected, dissolved in $CHCl_3$, and precipitated from

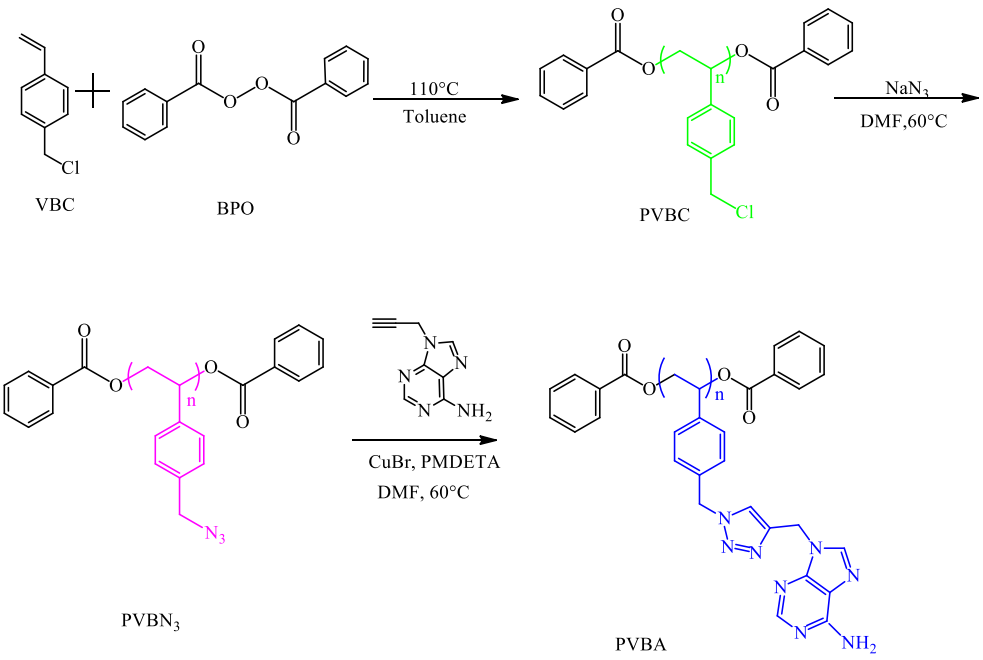

Scheme 1 Synthesis of the PVBA homopolymer from the VBC monomer through free radical polymerization, azidation, and a click reaction

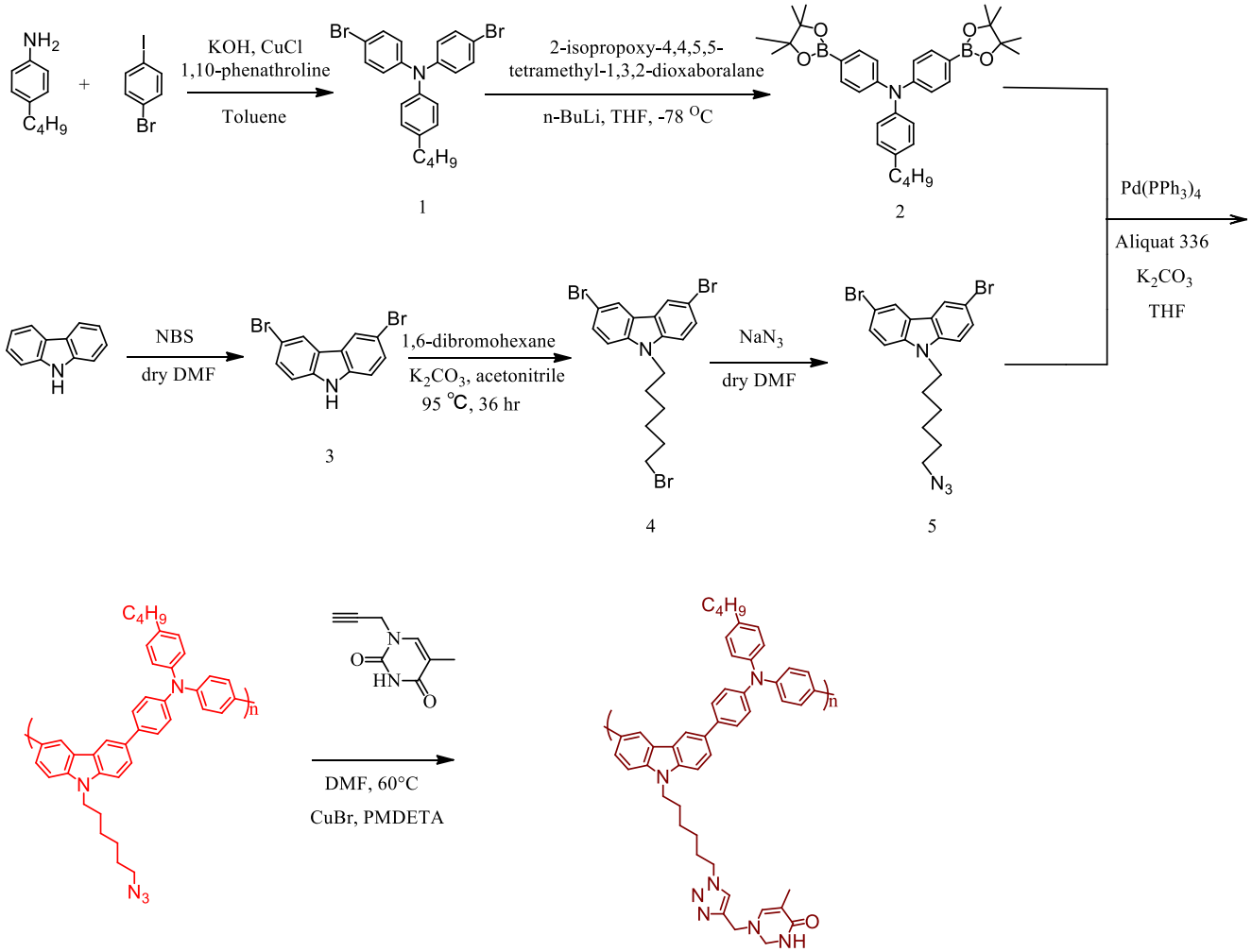

Scheme 2 Synthesis of the conjugated polymer PTC-T through Suzuki coupling polymerization and a click reaction

acetone several times to remove the catalyst and any possible monomer residues. The resulting PTC-N_3 copolymer was dried under vacuum to provide a brown solid (yield: 70%). Next, a mixture of PTC-N_3 (0.6 g, 1.1 mmol of N_3 units), PA (0.54 g, 3.4 mmol), and CuBr (8 mg) was subjected to the freeze/pump/thaw cycle. PMDETA (10 μL) was also added into a reaction vessel, which was heated at 50 °C for 24 h. This mixture was also passed through the aluminum oxide column and dialyzed with MeOH and dilute HCl. Three cycles of reprecipitation in MeOH given the PTC-T copolymer as a yellow powder (yield: 95%).

PVBA/PTC-T blend complexes

Various compositions of PVBA and PTC-T were dissolved in DMF solvent and then the blend solution was stirred for 3 days at room temperature. The DMF was then evaporated slowly at 90 °C under vacuum for 5 days.

Characterization

NMR spectra of samples in d_6-DMSO were recorded using a Varian Unity Inova 500 FT-NMR spectrometer operated at 500 MHz. FTIR spectroscopy was performed using the Bruker Tensor 27 FTIR spectrophotometer and the typical KBr disk method; 32 scans were collected at a spectral resolution of 1 cm^{-1}. The sample film was sufficiently thin to follow the Beer–Lambert law. The molecular weight and corresponding polydispersity were recorded by using gel permeation chromatography (GPC) at 80 °C; the Jasco PU-980 apparatus was equipped the UV and RI detectors; DMF was the eluent (flow rate: 0.6 mL/min). The glass transition temperatures of the PVBA/PTC-T blend samples were measured using a TA Q-20 instrument; the temperature was ramped from 25 to 250 °C at a heating rate of 20 °C/min under a N_2 atmosphere. UV–Vis absorption spectroscopy was performed using a Jasco V-770 spectrometer; the solution was placed in a small quartz cell (dimensions: 4.5 × 1.0 × 0.2 cm^3). The concentration of the blend sample in the organic solvent was

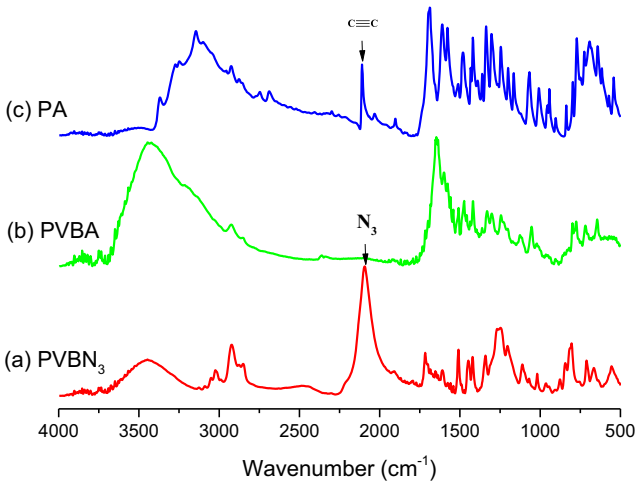

Fig. 1 FTIR spectra recorded at room temperature of **a** the $PVBN_3$ homopolymer, **b** the PVBA homopolymer, and **c** PA

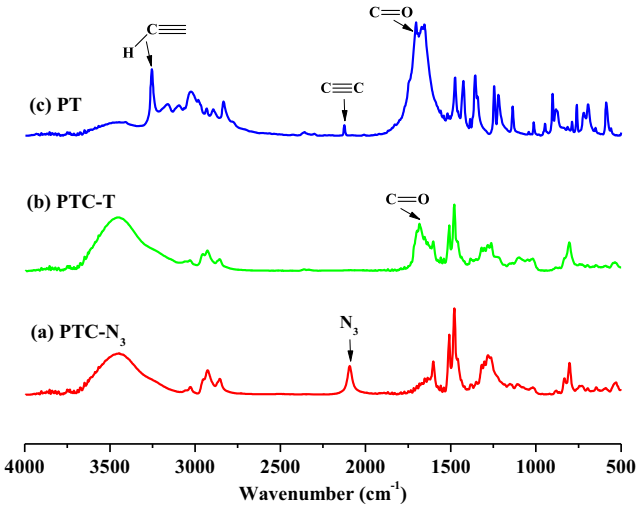

Fig. 3 FTIR spectra recorded at room temperature of **a** PTC-N_3 **b** PTC-T, and **c** PT

maintained at 10^{-4} M. Photoluminescence (PL) emission spectra were recorded from 200 to 800 nm using a LabGuide X350 fluorescence spectrometer and a Xe light source; the concentration of the blend sample was also 10^{-4} M range.

Results and discussion

Synthesis of PVBA and PTC-C

We used simple free radical polymerization to prepare the PVBC homopolymer, with BPO as the initiator for the thermal solution polymerization of the monomer VBC at 110 °C in toluene; we then converted the PVBC to the $PVBN_3$ homopolymer through treatment with NaN_3 [42]. The PVBA homopolymer was obtained after a click reaction of $PVBN_3$ with PA in a DMF solution containing PMDETA and CuBr (Scheme 1). Figure 1 displays the FTIR spectra of $PVBN_3$, PVBA, and PA, recorded at room temperature. The characteristic absorption band of the azido units at 2093 cm^{-1} was evident for the $PVBN_3$ homopolymer [Fig. 1(a)], with the C ≡ C absorption of PA located at 2106 cm^{-1} [Fig. 1(c)]. Both of these absorption bands disappeared after performing the click reaction of $PVBN_3$ with PA to form PVBA [Fig. 1(b)], suggesting that the N_3 and C ≡ C functionalities participated in this post-functionalization transformation. ^{1}H NMR spectra confirmed in the success of the reaction as displayed in Fig. 2. The signal for the CH_2 units adjacent to the side chain N_3 units of $PVBN_3$ appeared at 4.24 ppm [Fig. 2(a)]; this

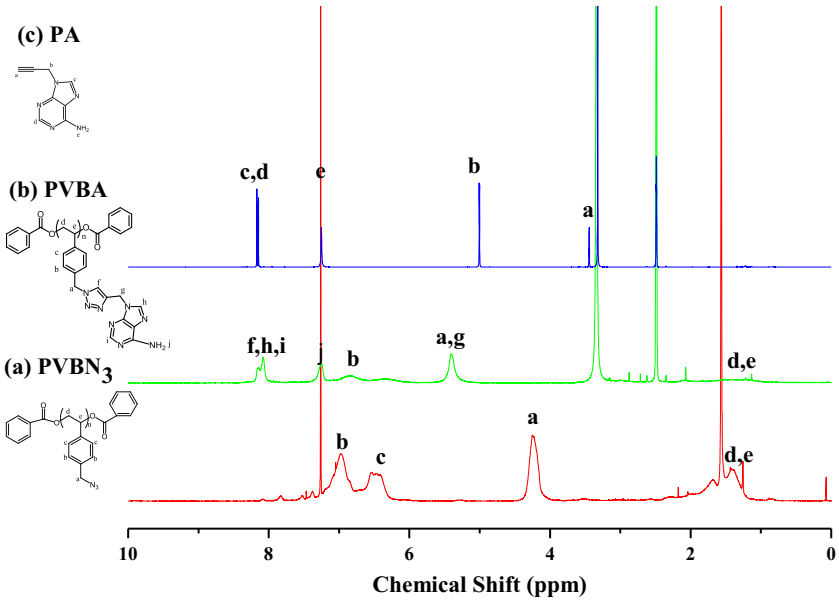

Fig. 2 ^{1}H NMR spectra and peak assignments of **a** the $PVBN_3$ homopolymer, **b** the PVBA homopolymer, and **c** PA

signal shifted to 5.41 ppm after the click reaction with PA [Fig. 2(b)]. The characteristic signals of PA appeared at 7.23 (NH_2) and 8.14–8.18 (aromatic protons) ppm. The signal for the H-C ≡ C unit of PA at 3.44 ppm disappeared and the signal for the CH_2 group adjacent to the A unit shifted from 5.00 ppm [Fig. 2(c)] to 5.41 ppm after the click reaction formed the PVBA homopolymer. The corresponding molecular weight (M_n) and PDI of the PVBA homopolymer, measured through GPC analysis, were 5700 and 1.56, respectively.

Similarly, we synthesized the PTC-T copolymer through the click reaction of the PTC-N_3 copolymer with PT (Scheme 2). Figure 3 presents the FTIR spectra of PTC-N_3, PTC-T, and PT, measured at room temperature. The signal for the side chain azido groups of PTC-N_3 appeared at 2093 cm^{-1}; the signals for the C=O and C≡C units of PT appeared at 1680 and 2123 cm^{-1}, respectively. The signals for the N_3 and C ≡ C units disappeared after performing the click reaction of PTC-N_3 with PT; the FTIR spectrum of PTC-T retained the signal for the C=O units of T group at 1680 cm^{-1}. NMR spectra confirmed the success of this click reaction. The signal for the CH_2 group adjacent to the side chain N_3 units was located at 3.22 ppm for PTC-N_3 [Fig. 4(a)]; it shifted to 4.25 ppm after the click reaction with PT [Fig. 4(b)]. Furthermore, the signals of the T unit of PT in d_6-DMSO appeared at 1.76 and 11.26 ppm, representing the CH_3 and NH units, respectively [Fig. 4(c)]; these signals remained in the spectrum of the PTC-T copolymer, whereas the signal for the C ≡ C units from PT, originally at 2.50 ppm, had disappeared. Taking into account all these data, we conclude that the PTC-T copolymer had been synthesized through the click reaction; GPC analysis provided a value of M_n of 16,800 and a PDI of 1.42.

Thermal analyses and multiple hydrogen bonding interaction of PVBA/PTC-T blends

DSC is a general method of thermal analysis for examining the miscibility behavior of polymer blends. Figure 5(b) displays DSC thermograms of PTC-T/PVBA blends of various compositions. For PTC-N_3, the glass transition temperature (T_g) was 109.4 °C (for brevity, not shown here). The thermogram for pure PTC-T exhibited a single value of T_g at 161.7 °C; we did not observe any obvious melting or crystallization peaks during the heating or cooling processes, suggesting the poor packing ability of the TPA units of the PTC-T copolymer. The relatively higher value of T_g for the PTC-T copolymer suggested that the strong multiple T···T interactions restricted the molecular motion and then decreased the free volume. Furthermore, the thermogram for the pure PVBA homopolymer exhibited its value of T_g at 169.1 °C; relative to that of PS (T_g = 100 °C), we attribute the significantly higher glass transition temperature to the strong hydrogen bonding of A···A binary pairs, which also restricted the molecular motion and decreased the free volume. A single value of T_g was observed for all of the PTC-T/PVBA blends, indicating that completely miscible blend formed the homogeneous phase. Furthermore, each single T_g value was greater than those of

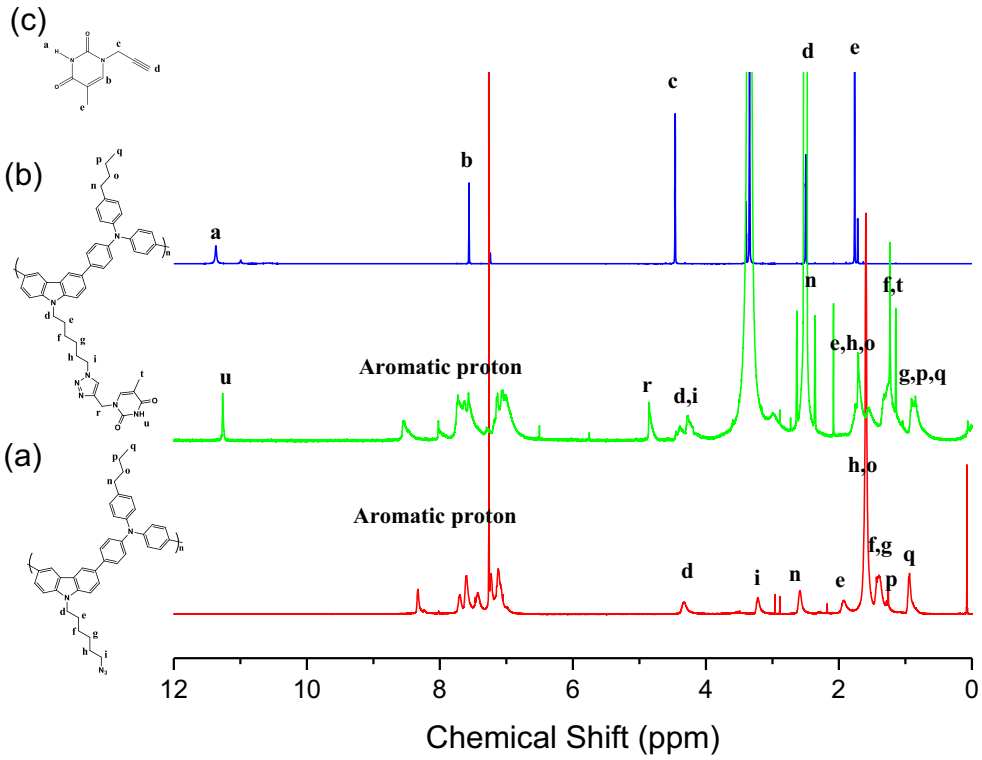

Fig. 4 ^{1}H NMR spectra and peak assignments of **a** the PTC-N_3 homopolymer, **b** PTC-T, and **c** PT

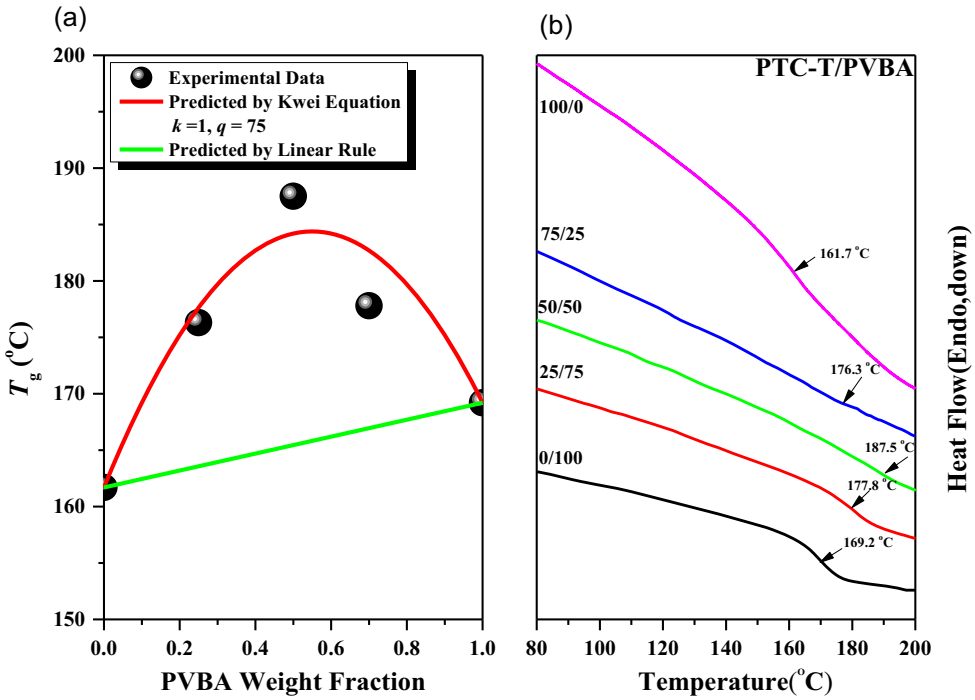

Fig. 5 **a** Glass transition temperature behavior of PTC-T/PVBA blends, based on Kwei equation. **b** DSC thermograms of PTC-T/PVBA blends with various compositions, recorded during the second heating scans

both the individual PTC-T and PVBA polymers; the large positive deviation from the linear rule is consistent with strong intermolecular A···T hydrogen bonding between these two polymers. The Kwei equation is typically used to predict the glass transition temperatures of miscible polymer blends system featuring strong intermolecular interactions [43]:

$$T_g = \frac{W_1 T_{g1} + kW_2 T_{g2}}{W_1 + kW_2} + qW_1 W_2 \quad (1)$$

where W_i is the weight fraction, T_{gi} represents the glass transition temperature of PTC-T or PVBA, and k and q are fitting constants. The fitting results displayed in Fig. 5(a) reveal that the highest value of T_g was that (187.5 °C) for the PTC-T/PVBA = 50/50 blend. This value was approximately 26 °C higher than that of the pure PTC-T. Scheme 3 depicts the possible physical crosslinking, induced by multiple hydrogen bonding, in the supramolecular structure of the PTC-T/PVBA complex. Furthermore, we obtained the values of k and q of 1 and 75, respectively, based on nonlinear least-squares best-fit analysis. The positive value of q indicated that strong intermolecular interactions in the PTC-T/PVBA complex system were directly responsible for the significantly increases in the T_g values of the blends.

In general, such multiple hydrogen bonding interactions can also be characterized using NMR and FTIR spectroscopy. In previous studies [31, 44], we used ^{1}H NMR spectroscopic titration to characterize VBT/VBA and AC-16/TC-16 binary pairs, obtaining an inter-association equilibrium constant (K_a) of 534 M^{-1} for the monomer in $CDCl_3$ [31]; we examined these monomers because the PVBA or PTC-T polymers could not dissolve in such a low-polarity solvent. Here, we monitored the PTC-T/PVBA complex directly in d_6-DMSO to examine its inter-association behavior. As mentioned above, the signal for the NH units in PTC-T was located at 11.26 ppm [Fig. 6(a)]; this signal shifted downfield slightly to 11.30 ppm in the presence of 75 wt% PVBA [Fig. 6(d)]. In addition, the signal for the NH_2 units in PVBA was located at 7.26 ppm

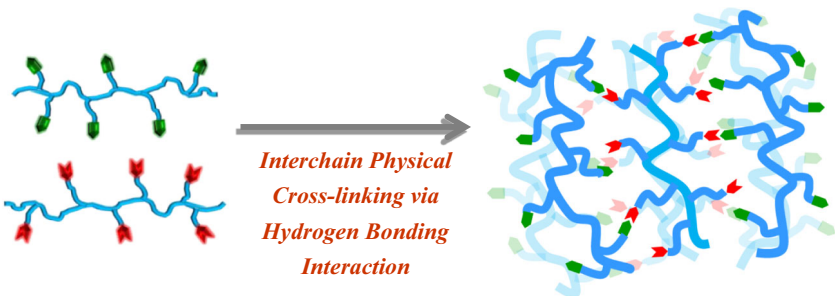

Scheme 3 Schematic representation of inter-chain physical crosslinking in the PTC-T/PVBA supramolecular complex, stabilized through multiple hydrogen bonding interactions

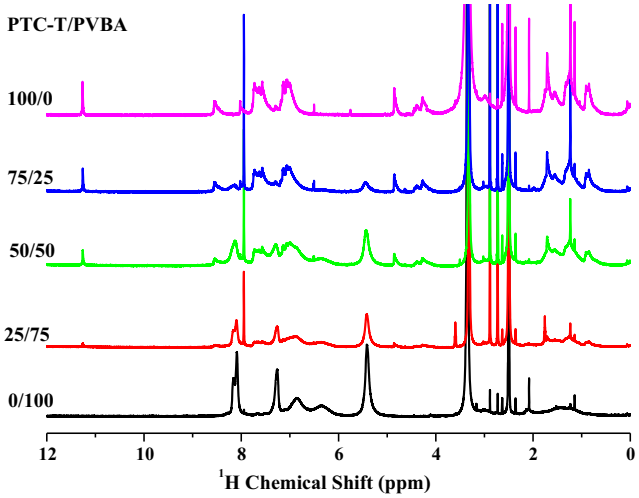

Fig. 6 ^{1}H NMR spectra of PTC-T/PVBA blends of various compositions as solutions in d_6-DMSO

[Fig. 6(e)]; this signal also shifted downfield to 7.30 ppm [Fig. 6(b)], consistent with complementary multiple hydrogen bonding occurring in the PTC-T/PVBA blend system. Because the pure PTC-T and PVBA dissolved both only in *d*-DMSO, a highly polar solvent, the changes in chemical shift and the value of K_a would be smaller than those obtained previously using model compounds in $CDCl_3$ solution [44].

FTIR spectral analysis is also another useful characterization for understanding the multiple hydrogen bonding in the solid state to eliminate the effects of solvents. Figure 7(a) displays FTIR spectra of the PTC-T/PVBA blend system, measured at room temperature. A broad absorption signal appeared for NH stretching in the range from 3200 to 3600 cm^{-1}. The signal for the free NH units appeared near 3445 cm^{-1}; this band shifted at 3320 cm^{-1} when the A interacted with the T groups. Furthermore, the signal appeared at 3180 cm^{-1}, corresponding to the NH absorption of the T interacting with the A units [45–47]. Figure 7(b) presents the C=O absorption signals of PTC-T blended with the PVBA homopolymer. The spectrum of the pure PTC-T exhibited several major peaks, including (i) signals for multiple hydrogen bonded and free $C_4=O$ groups of the T units of PTC-T, at 1668 and 1681 cm^{-1}, respectively, and (ii) a signal for the free $C_2=O$ groups of the T units of PTC-T at 1711 cm^{-1} [45–47]. The characteristic signal of PVBA was located at 1642 cm^{-1}, due to the NH_2 scissor vibration. Because the signals for the multiple hydrogen bonding of the T and A units were located between 1665 and 1655 cm^{-1}, it was difficult to measure the area fraction of each peak; instead, we paid attention only to the area fraction of the signal for the free $C_2=O$ groups at 1711 cm^{-1}. This area fraction decreased from 0.33 for the free $C_2=O$ groups of the pure PTC-T to 0.12 for PTC-T/PVBA = 25/75, consistent with the presence of multiple hydrogen bonding between T and A units in the PTC-T/PVBA blend systems.

UV and PL spectral analyses of PTC-T/PVBA blends

We used UV and PL spectra to examine the absorption and emission properties of the PTC-T/PVBA blends. Figure 8(a) displays the UV spectra of the PTC-T/PVBA blends in DMF at a concentration of 10^{-4} M. The UV absorption intensity of PTC-T decreased upon increasing the concentration of PVBA in the blend system, as expected; the maximum absorption

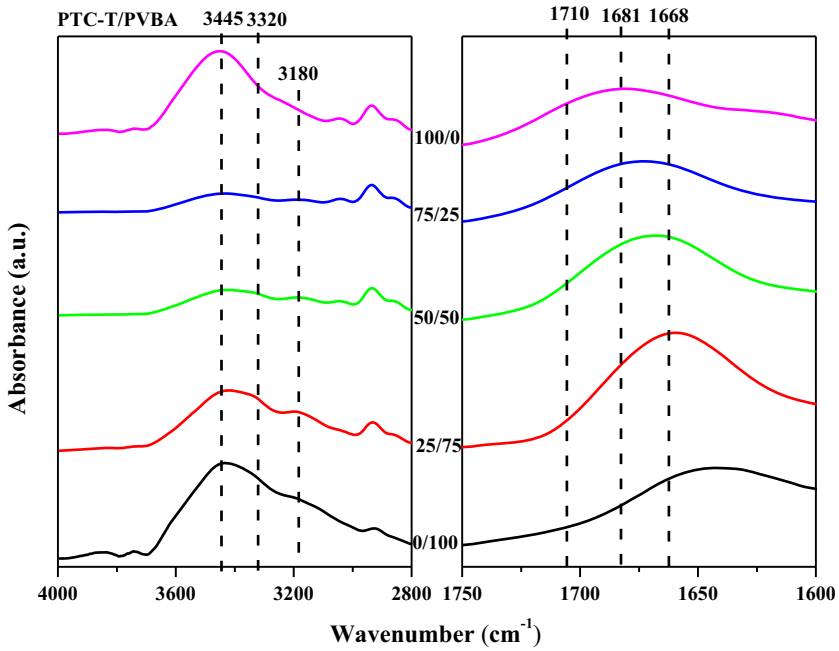

Fig. 7 FTIR spectra of PTC-T/PVBA blends of various compositions, recorded at room temperature

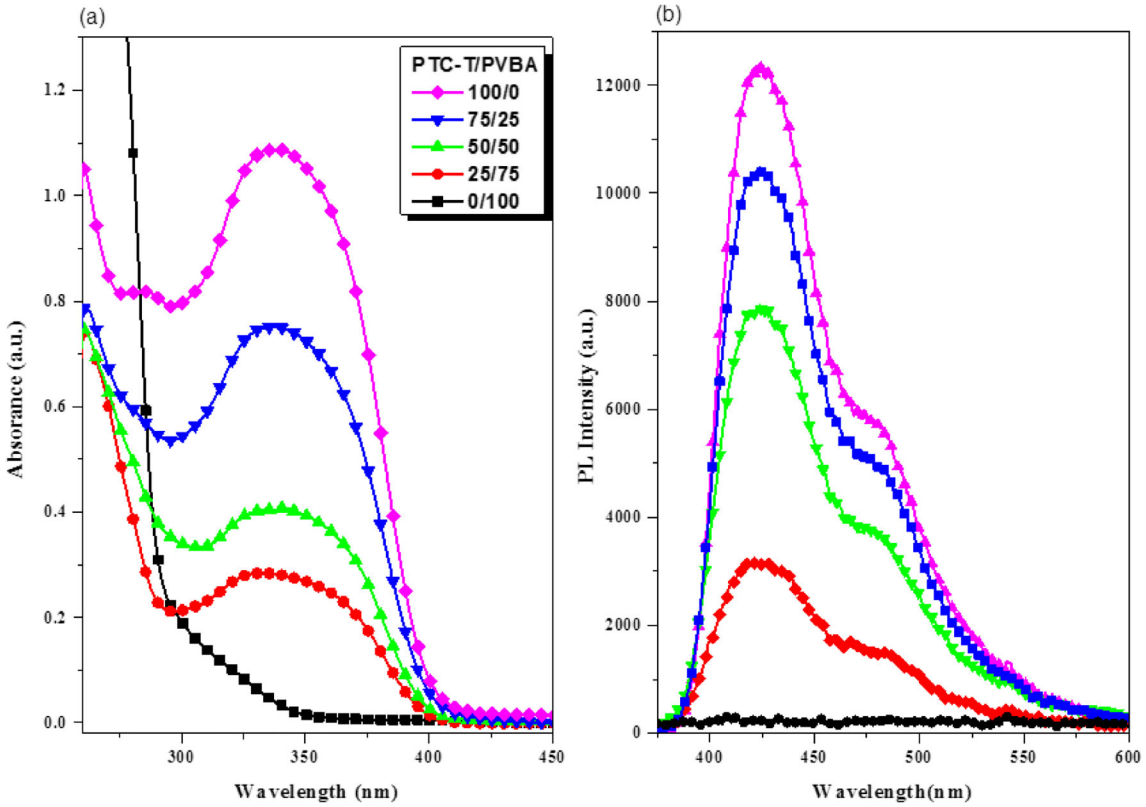

Fig. 8 **a** UV and **b** PL spectra of PTC-T/PVBA blends of various compositions, recorded at room temperature

length of 337.5 nm for the pure PTC-T became broad and red-shifted upon increasing the concentration of PVBA, indicative of the multiple hydrogen bonding in the blend system inducing the red-shift through polymer chain restriction. Figure 8(b) presents PL spectra of the PTC-T/PVBA blends in DMF at a concentration of 10^{-4} M, with a wavelength of 350 nm selected for excitation. The quantum yield, calculated based on the PL spectra, was highest (0.1109) for the blend PTC-T/PVBA = 50 /50 (cf. values of 0.0763 and 0.0792 for the PTC-T/PVBA = 75/25 and 25/75 blends, respectively), consistent with polymer chain restriction enhancing the quantum yield through the strong hydrogen bonding interactions [48].

Conclusion

We have used Suzuki coupling, free radical polymerization, and click reactions to synthesize a T-functionalized conjugated polymer (PTC-T) and an A-functionalized homopolymer (PVBA). These PTC-T/PVBA blends exhibited a single glass transition temperature at each composition, suggesting that their miscibility arose from strong complementary multiple hydrogen bonding of their A···T binary pairs. Furthermore, PL spectroscopy indicated that the photophysical properties of the luminescent PTC-T/PVBA blend films were strongly affected by the presence of these multiple hydrogen bonding interactions inducing physically crosslinked structures, with improvements in quantum yields arising from the phase-miscible behavior.

Acknowledgments This study was supported financially by the Ministry of Science and Technology, Taiwan, under contracts MOST 106-2221-E-110-067-MY3 and 105-2221-E-110-092-MY3.

References

1. Kim GH, Lee D, Shanker A, Kwon MS, Gidley D, Kim J, Pipe KP (2015) High thermal conductivity in amorphous polymer blends by engineered interchain interactions. Nat Mater 14:295–300
2. Kim T, Kim JH, Kang TE, Lee C, Kang H, Shin M, Wang C, Ma B, Jeong U, Kim TS, Kim BJ (2015) Flexible, highly efficient all-polymer solar cells. Nat Commun 6:8547
3. Lai SM, Liu YH, Huang CT, Don TM (2017) Miscibility and toughness improvement of poly(lactic acid)/poly(3-Hydroxybutyrate) blends using a melt-induced degradation approach. J Polym Res 24:102
4. Brown EA, Rider DA (2017) Pegylated Polybenzoxazine networks with increased thermal stability from miscible blends of Tosylated poly(ethylene glycol) and a Benzoxazine monomer. Macromolecules 50:6468–6481
5. Lu SY, Lin YC, Kuo SW (2012) Separated coil and chain aggregation behaviors on the miscibility and helical peptide secondary structure of poly(tyrosine) with poly(4-vinyl pyridine). Macromolecules 45:6457–6556

6. Deimede V, Voyiatzis GA, Kallitsis JK, Qingfeng L, Bjerrum NJ (2000) Miscibility behavior of polybenzimidazole/sulfonated polysulfone blends for use in fuel cell applications. Macromolecules 33:7609–7617
7. Don TM, Liao KH (2018) Studies on the alcoholysis of poly(3-hydroxybutyrate) and the synthesis of PHB-b-PLA block copolymer for the preparation of PLA/PHB-b-PLA blends. J Polym Res 25:38
8. Coleman MM, Painter PC (1995) Hydrogen Bonded Polymer blends. Prog Polym Sci 20:1–59
9. Kuo SW (2008) Hydrogen-Bonding in Polymer Blends. J Polym Res 15:459–486
10. Kuo SW (2012) Miscibility enhancement of polymer blends through multiple hydrogen bonding interactions. In functional polymer blends: synthesis, properties and performance, Ed. Vikas Mittal, Taylor & Francis, Chapter 2, 27–52
11. Tsai CC, Gan Z, Chen T, Kuo SW (2018) Competitive hydrogen bonding interactions influence the secondary and hierarchical self-assembled structures of polypeptide-based triblock copolymers. Macromolecules 51:3017–3029
12. Flory PJ (1978) Statistical thermodynamics of mixtures of rodlike particles. 5. Mixtures with random coils. Macromolecules 11:1138–1141
13. Adams M, Dogic Z, Keller SL, Farden S (1998) Entropically driven microphase transitions in mixtures of colloidal rods and spheres. Nature 393:349–352
14. Heitz T, Rohrback P, Hocker H (1989) Rigid rods with flexible side chains-A route to molecular reinforcement? Macromol Chem 190: 3295–3316
15. Jenekhe SA, Chen XL (1999) Self-assembly of ordered microporous materials from rod-coil block copolymers. Science 283:372–375
16. Lee M, Cho BK, Zin WC (2001) Supramolecular structures from rod−coil block copolymers. Chem Rev 101:3869–3892
17. Ince O, Akyol E, Sulu E, Sanal T, Hazer B (2015) Synthesis and characterization of novel rod-coil (tadpole) poly(linoleic acid) based graft copolymers. J Polym Res 23:5
18. Nguyen TH, Nguyen LTT, Nguyen VQ, Phan LNT, Zhang G, Yokozawa T, Phung DTT, Nguyen HT (2018) Synthesis of poly(3-hexylthiophene) based rod–coil conjugated block copolymers via photoinduced metal-free atom transfer radical polymerization. Polym Chem 9:2484
19. Kuo SW, Chen CJ (2011) Using hydrogen bonding interactions to control the peptide secondary structures and miscibility behavior of poly(L-glutamates)s with phenolic resin. Macromolecules 44: 7315–7326
20. Kuo SW, Chen CJ (2012) Functional polystyrene derivatives influence the miscibility and helical peptide secondary structures of poly(benzyl L-glutamate). Macromolecules 45:2442–2452
21. Lu SY, Kuo SW (2015) Miscible polypeptide blends of Polytyrosine and poly(γ-methyl L-glutamate) with rigid-rod conformations. RSC Adv 5:88539–88547
22. Cambridge G, Gonzalez-Alvarez MJ, Guerin G, Manners I, Winnik MA (2015) Solution self-assembly of blends of crystalline-coil Polyferrocenylsilane-block-polyisoprene with Crystallizable Polyferrocenylsilane Homopolymer. Macromolecules 48:707–716
23. Mohamed MG, Cheng CC, Lin YC, Huang CW, Lu FH, Chang FC, Kuo SW (2014) Synthesis and self-assembly of water soluble Polythiophene-grafted-poly(ethylene oxide) copolymers. RSC Adv 4:21830–21839
24. Lu FH, Mohamed MG, Liu TF, Chao CC, Kuo SW (2015) A facile Cosolvent/chelation method for the preparation of semi-crystalline $CuCl_2$(ethylene glycol)/poly(3-hexylthiophene) complexes displaying specific luminescence properties. RSC Adv 5:87723–87729
25. Salunkhe PH, Patil YS, Patil VB, Navale YH, Dhole IA, Ubale VP, Maldar NN, Ghanwat AA (2018) Synthesis and characterization of conjugated porous polyazomethines with excellent electrochemical energy storage performance. J Polym Res 25:147
26. Liu S, He P, Hussain S, Lu H, Zhou X, Lu F, Liu L, Dai Z, Wang S (2018) Conjugated polymer-based Photoelectrochemical Cytosensor with turn-on enable signal for sensitive cell detection. ACS Appl Mater Interfaces 10:6618–6623
27. Wang YS, Cheng CC, Ye YS, Yen YC, Chang FC (2012) Bioinspired photo-cross-linked nanofibers from uracil-functionalized polymers. ACS Macro Lett 1:159–162
28. Wang YS, Cheng CC, Chen JK, Ko FH, Chang FC (2013) Bioinspired supramolecular fibers for mercury ion adsorption. J Mater Chem A 1:7745–7750
29. Vohra V, Giovanella U, Tubino R, Murata H, Botta C (2011) Electroluminescence from conjugated polymer electrospun nanofibers in solution processable organic light-emitting diodes. ACS Nano 5:5572–5578
30. Xin Y, Huang ZH, Yan EY, Zhang W, Zhao Q (2006) Controlling poly(−phenylene vinylene)/poly(vinyl pyrrolidone) composite nanofibers in different morphologies by electrospinning. Appl Phys Lett 89:053101
31. Kuo SW, Cheng RS (2009) DNA-like interactions enhance the miscibility of supramolecular polymer blends. Polymer 50:177–188
32. Kuo SW, Tsai ST (2009) Complementary multiple hydrogen-bonding interactions increase the glass transition temperatures to PMMA copolymer mixtures. Macromolecules 42:4701–4711
33. Kuo SW, Hsu CH (2010) Miscibility enhancement of supramolecular polymer blends through complementary multiple hydrogen bonding interactions. Polym Int 59:998–1005
34. Wu YC, Kuo SW (2012) Complementary multiple hydrogen bonding interactions mediate the self-assembly of supramolecular structures from thymine-containing block copolymers and Hexadecyladenine. Polym Chem 3:3100–3111
35. Wu YC, Bastakoti BP, Pramanik M, Yamauchi Y, Kuo SW (2015) Multiple hydrogen bonding mediates the formation of multicompartment micelles and hierarchical self-assembled structures from pseudo A-block-(B-graft-C) terpolymers. Polym Chem 6:5110–5124
36. Huang CW, Wu PW, Su WH, Zhu CY, Kuo SW (2016) Stimuli-responsive supramolecular materials: photo-tunable and molecular recognition behavior. Polym Chem 7:795–806
37. Su WJ, Wu YS, Wang CF, Kuo SW (2018) Self-assembled structures of Diblock copolymer/Homopolymer blends through multiple complementary hydrogen bonds. Crystals 8:330
38. Huang KW, Wu YR, Kuo SW (2013) From random coil polymers to helical structures induced by carbon nanotubes and supramolecular interactions. Macromol Rapid Commun 34:1530–1536
39. Huang CW, Chang FC, Chu YL, Lai CC, Lin TE, Zhu CY, Kuo SW (2015) A solvent-resistant Azide-based hole injection/transporting conjugated polymer for fluorescence and phosphorescence light-emitting diodes. J Mater Chem C 3:8142–8151
40. Huang CW, Ji WY, Kuo SW (2017) Water-soluble fluorescent nanoparticles from supramolecular Amphiphiles featuring Heterocomplementary multiple hydrogen Bondings. Macromolecules 50:7091–7101
41. Huang CW, Ji WY, Kuo SW (2018) Stimuli-responsive supramolecular conjugated polymer with Phototunable surface relief grating. Polym Chem 9:2813–2820
42. Huang KW, Kuo SW (2013) High-Heteronucleobase-content polystyrene copolymers prepared using click chemistry form supramolecular structures with melamine through complementary multiple hydrogen-bonding interactions. Macromol Chem Phys 213:1509–1519

43. Kwei T (1984) The effect of hydrogen bonding on the glass transition temperatures of polymer mixtures. J Polym Sci Polym Lett Ed 22:307–313
44. Wu YS, Wu YC, Kuo SW (2014) Thymine- and adenine-functionalized polystyrene form self-assembled structures through multiple complementary hydrogen bonds. Polymers 6:1827–1845
45. Yamauchi K, Kanomata A, Inoue T, Long TE (2004) Thermoreversible polyesters consisting of multiple hydrogen bonding (MHB). Macromolecules 37:3519–3522
46. Garcia M, Beecham MP, Kempe K, Haddleton DM, Khan A, Marsh A (2015) Water soluble triblock and pentablock poly(methacryloyl nucleosides) from copper-mediated living radical polymerisation using peg macroinitiators. Eur Polym J 66:444–451
47. Cheng CC, Huang CF, Yen YC, Chang FC (2008) A "plug and play" polymer through biocomplementary hydrogen bonding. J Polym Sci A Polym Chem 46:6416–6424
48. Cheng CC, Wang YS, Chang FC, Lee DJ, Yang LC, Chen JK (2015) Supramolecular assembly-induced enhanced emission of electrospun nanofibers. Chem Commun 51:672–675